

Dynamics of vibrationally excited ozone formed by threebody recombination. II. Kinetics and mechanism

W. T. Rawlins, G. E. Caledonia, and R. A. Armstrong

Citation: *J. Chem. Phys.* **87**, 5209 (1987); doi: 10.1063/1.453689

View online: <http://dx.doi.org/10.1063/1.453689>

View Table of Contents: <http://jcp.aip.org/resource/1/JCPSA6/v87/i9>

Published by the [American Institute of Physics](#).

Additional information on *J. Chem. Phys.*

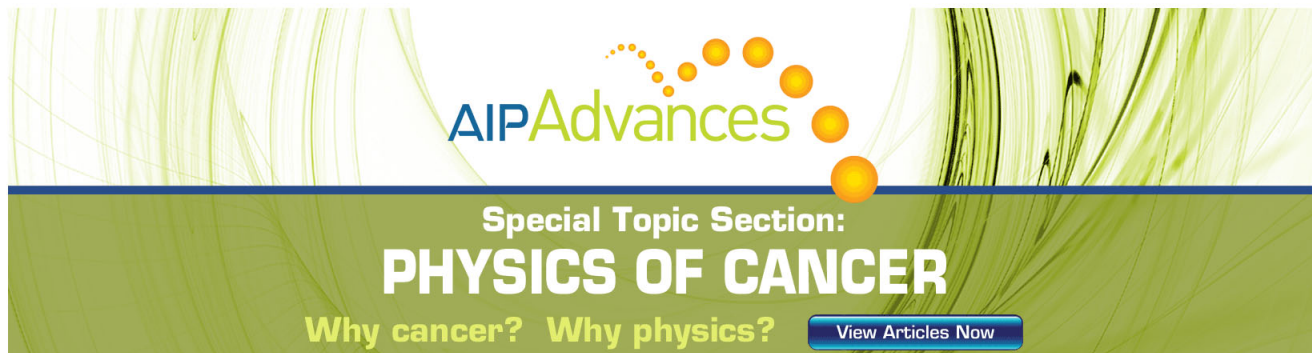
Journal Homepage: <http://jcp.aip.org/>

Journal Information: http://jcp.aip.org/about/about_the_journal

Top downloads: http://jcp.aip.org/features/most_downloaded

Information for Authors: <http://jcp.aip.org/authors>

ADVERTISEMENT



AIP Advances

Special Topic Section:
PHYSICS OF CANCER

Why cancer? Why physics? [View Articles Now](#)

Dynamics of vibrationally excited ozone formed by three-body recombination. II. Kinetics and mechanism

W. T. Rawlins and G. E. Caledonia

Physical Sciences Inc., Research Park, P. O. Box 3100, Andover, Massachusetts 01810

R. A. Armstrong^{a)}

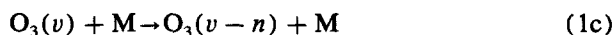
Infrared Technology Division, Air Force Geophysics Laboratory, Hanscom AFB, Massachusetts 01731

(Received 19 June 1987; accepted 21 July 1987)

Spectrally resolved infrared chemiluminescence from vibrationally excited ozone, $O_3(v)$, has been used to study the reaction kinetics of $O_3(v)$ in discharged O_2/Ar mixtures at ~ 1 Torr and 80–150 K. Dependences of the excited state number densities on temperature and O_2 mole fraction indicate $O_3(v)$ is formed primarily by three-body recombination of O with O_2 and is destroyed by rapid chemical reaction with O. Several secondary excitation reactions involving vibrationally and electronically excited O_2 are also indicated. The data are treated with a detailed steady-state analysis of the discharge kinetics, to extract estimates for rate coefficients of the key elementary reactions. The effective “quasinascent” state distribution in recombination is also inferred; this distribution shows selective recombination into the asymmetric stretching mode, but an apparently statistical (i.e., collisionally scrambled) behavior among the vibrational states within that mode. The results are discussed in terms of the detailed dynamics of three-body recombination.

I. INTRODUCTION

The chemical kinetics of vibrationally excited ozone, $O_3(v)$, is a complex problem of fundamental importance in studies of atmospheric photochemistry as well as in basic molecular dynamics. Experimental observations of $O_3(v)$ formed during the three-body recombination sequence



can provide insight to the detailed dynamics of the initial formation of $O_3(v)$ and to the subsequent vibrational deactivation and intermode exchange. In particular, low-pressure observations of discrete $O_3(v)$ states formed in early stages of the recombination sequence can provide a unique data base on a marginally understood problem in chemical kinetics: the molecular dynamics and mechanisms of recombination and energy transfer in polyatomic systems.¹

The kinetics of $O_3(v)$ formation and deactivation have been addressed by a number of investigators. In general, $O_3(v)$ is usually formed by laser excitation of the ν_3 mode or by three-body recombination following flash photolysis, and is detected by ultraviolet absorption or broadband infrared fluorescence. Rosen and Cool²⁻⁴ studied the quenching of infrared fluorescence from low-lying, laser-excited vibrational states of O_3 by several reagents, and showed that vibration-to-translation ($V \rightarrow T$) energy transfer near the bottom of the potential well is rate limited by deactivation from the well-coupled symmetric (ν_1) and asymmetric (ν_3) stretching modes through the poorly coupled bending (ν_2) mode. Using similar techniques, West *et al.*^{5,6} studied the deactivation of low levels of $O_3(v)$ by O, concluding that the deactivation pathway was primarily $V \rightarrow T$ energy transfer rather than chemical conversion to O_2 .

von Rosenberg and Trainor⁷⁻⁹ were the first to observe $O_3(v)$ formed in three-body recombination, reporting on the production and deactivation of broadband infrared fluorescence in the ν_3 , $\nu_1 + \nu_3$, and ν_2 bands. Working at total pressures of 100 to 400 Torr, they found greater excitation in the bending than in the stretching modes, presumably because of the extensive collisional deactivation and intermode transfer by both $V \rightarrow T$ and $V \rightarrow V$ [$O_3(v) + O_3$ intermode equilibration] processes that occurred under these conditions. More recently, the kinetics of laser-initiated and recombination-generated $O_3(v)$ have been reinvestigated using ultraviolet absorption in the Hartley bands as the diagnostic for $O_3(v)$.¹⁰⁻¹⁵ These studies are somewhat less definitive than the infrared fluorescence measurements owing to the greater difficulty of resolving contributions from different modes to the observed absorption spectra. However, the results are generally consistent with the analogous infrared fluorescence data. It is noteworthy that Joens *et al.*,¹⁵ investigating recombination under conditions of $V \rightarrow T$ -dominated collisional deactivation, inferred initial formation of $O_3(v)$ in the stretching modes followed by kinetically limited collisional transfer to the bending mode, in contrast to the results of von Rosenberg and Trainor.⁷⁻⁹

Except for the $O + O_3(v)$ studies,^{5,6} all of the above experiments were performed in a flash-photolysis mode, with relatively high pressures of order 10^2 Torr, observation times of 10 to 100 μs , and room temperature. Thus the newly formed $O_3(v)$ molecules experienced on the order of 10^4 – 10^6 collisions on the time scale of the observations. In many cases, O_3 was a significant collision partner, providing the avenue of rapid $V \rightarrow V$ equilibration. In contrast, in the upper atmosphere [e.g., altitudes of 80 to 100 km, where $O_3(v)$ effects are most pronounced], an excited $O_3(v)$ molecule

^{a)} Present address: Mission Research Corporation, 1 Tara Blvd., Suite 302, Nashua, NH 03062.

suffers only about 10^2 – 10^3 collisions in the time scale of its radiative lifetime; the principal collision partners are N_2 and O_2 , which we expect to induce simple $V \rightarrow T$ cascade down the vibrational ladder, and O , which may give more complex deactivation pathways. Thus it is important to probe the earliest possible stages of the recombination sequence, where the effects of $V \rightarrow T$ cascade [reaction (1c)] are minimized, in order to determine the range of vibrational levels which are likely to be populated in high-altitude atmospheric conditions.

We report here on studies of the $O + O_2$ recombination sequence in flowing, microwave-discharged O_2/Ar mixtures near 1 Torr and at low temperatures, 80 to 150 K. Prior to their observation, the $O_3(v)$ molecules experience $\sim 10^4$ collisions, primarily with Ar, a relatively inefficient $V \rightarrow T$ transfer partner. Thus collisional effects are significant but are not severe enough to destroy information about the early stages of the recombination sequence. The measurements were made by directly observing the spectrally resolved infrared chemiluminescence from $O_3(v)$ in the ν_3 band near $10 \mu m$, using the cryogenic COCHISE (cold chemiexcitation infrared stimulation experiment) infrared reactor/spectrometer facility¹⁶ at the Air Force Geophysics Laboratory. Our earlier investigation,¹⁷ with a limited set of experimental conditions, produced the first laboratory spectra of $O_3(v)$ fluorescence, attributed this fluorescence to three-body recombination in steady state with collisional deactivation, demonstrated the effects of deactivation by atomic oxygen, and hinted at the possibility of other discharge-related excitation mechanisms. We have now reinvestigated this problem with greater dynamic range so that more definitive conclusions can be made regarding both spectroscopic and kinetic/mechanistic issues which arose in the earlier work. The detailed spectroscopic observations have been reported in a companion paper (paper I).¹⁸ We report here on the results and interpretations of kinetic/spectroscopic experiments whose objectives are to: (1) determine a quasiinitial state distribution from the recombination reaction, for use in atmospheric modeling; (2) assess the kinetic effects of deactivation by atomic oxygen; and (3) characterize and identify other $O_3(v)$ excitation mechanisms arising in the discharged gas. The results of this work are generally consistent with those from the initial studies,¹⁷ and serve to validate and extend our interpretations^{19–21} of the high-altitude chemistry of vibrationally excited ozone.

II. EXPERIMENTS AND SPECTRAL DATA

The COCHISE facility is described in detail elsewhere,¹⁶ and the configuration of the $O_3(v)$ experiments is described thoroughly in paper I.¹⁸ $O_3(v)$ is produced in four parallel microwave discharges (2450 MHz, 50 W) of rapidly flowing O_2/Ar mixtures at ~ 1 Torr total pressure and selected temperatures between 80 and 150 K. The discharge effluents expand into a low-pressure (~ 3 mTorr), cryogenically pumped chamber, where they enter the collimated field of view of a scanning monochromator/infrared detector assembly. Optional opposing flows of O_2 or Ar may be used to create a quasistatic interaction region along the centerline of the field of view. The use of this counterflow thus gives some

increase in the observed effluent fluorescence intensities, but also causes partial rethermalization of the expansion-cooled rotational distributions. Thus in most of the experiments, counterflows were not employed in order to keep the rotational temperatures lower and minimize spectral overlap. The use of O_2 , Ar, and N_2 counterflows give essentially identical results; the absence of a counterflow gives the same vibrational spectral distributions but colder rotational distributions and about half the total intensity. These results confirm the expectation that measurable $O_3(v)$ is formed only in the discharge tubes and not in the low-pressure viewing region. Typical gas residence times are ~ 2 ms for the high-pressure (1 Torr) discharge region, 0.5 ms for the expansion region between the discharge exit and the field of view, and ~ 0.3 ms for the viewing volume.

Vibraluminescence from $O_3(v)$ was observed with spectral resolutions of 0.027 to $0.080 \mu m$ (2.7 to 8.0 cm^{-1}). For convenience and optimized signal-to-noise (S/N) ratio, the lower resolution was employed for most of the measurements. Higher resolution scans for selected conditions were used to develop and verify the spectroscopic model used in the analysis as described in paper I.¹⁸

The primary thrust of these experiments is to examine the variation in $O_3(v)$ number densities and relative population distributions with varying O_2 mole fraction in the discharge gas. Our previous work¹⁷ showed: (1) at low O_2 mole fractions, $\chi_{O_2} \leq 10^{-2}$, the relative contributions of the higher-lying states increased as χ_{O_2} decreased, presumably due to reduced collisional deactivation by atomic oxygen formed in the discharge; and (2) for $\chi_{O_2} \sim 10^{-1}$, bimodal vibrational distributions were obtained, implying the onset of another excitation reaction pumping the higher vibrational states. Accordingly, in the present experiments, the Ar flow rate was maintained at $640 \mu mol \text{ s}^{-1}$ and the O_2 flow rate was varied from 2.3 to $86 \mu mol \text{ s}^{-1}$ (0.3% to 12% O_2), all at a constant discharge tube temperature of 80 K. The dynamic range of χ_{O_2} was limited by poor S/N at the low end and difficulty of remote discharge ignition (inside the cryogenic chamber) at the upper end of the range. The variations in spectral distribution over this range are illustrated in Fig. 1.

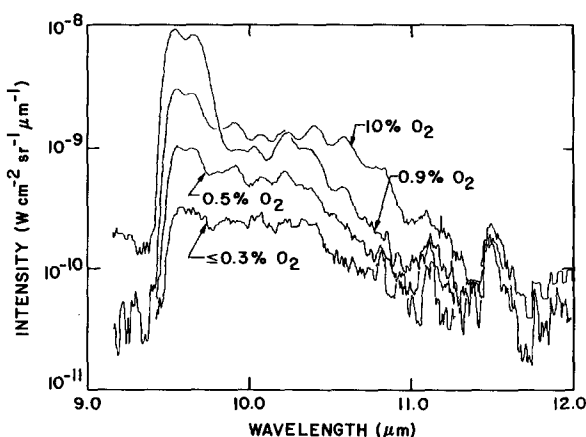


FIG. 1. Effect of O_2 level in discharged O_2/Ar mixtures on observed spectral distributions (no counterflow, 80 K, $640 \mu mol/s$ Ar, $0.08 \mu m$ resolution).

For selected constant O_2 and Ar flow velocities, the discharge sidearm and gas supply temperatures were varied systematically from 80 to 150 K. The effect on the observed spectra is illustrated in Fig. 2. The spectral distribution is seen to be invariant with temperature, however, the total intensity exhibits a strong negative temperature coefficient. These data lend credence to the interpretation that the observed $O_3(\nu)$ derives either directly or indirectly from ozone formed in three-body recombination, which follows a similar temperature dependence.²² We will pursue this point further in the next section.

Prior to analysis of the spectral data, it was necessary to correct the observed spectra for atomic argon Rydberg lines appearing as scattered light from the discharge tubes.²³ This was a straightforward procedure involving subtraction of background spectra obtained with no O_2 added to the discharges. This contamination was at worst only a minor effect near 10.0 and 10.3 μm , with stronger features near 11.1, 11.4, and 12.3 μm lying generally beyond the maximum spectral extent of the $O_3(\nu)$ emission.

During the course of the measurements, spectral surveys were conducted over the entire 2 to 16 μm range of the apparatus in search of other ozone emission bands besides the prominent ν_3 band reported here. The only other O_3 -related feature we could detect was the $\nu_1 + \nu_3$ combination band, which originates near 4.7 μm . The ν_1 and ν_2 bands, which are factors of 22 and 45 weaker than ν_3 ,²⁴ were not observable under any conditions of flow, temperature, or spectral resolution. Based on blackbody calibrations of the spectral responsivity, examination of the S/N of the ν_3 data, and the results of the spectral fitting analysis described below, we estimate a minimum detection limit for $O_3(001)$ of 5×10^6 molecules cm^{-3} , which in turn corresponds to detection limits of 1×10^8 and 3×10^8 cm^{-3} for $O_3(100)$ and $O_3(010)$, respectively. Also unobservable was any O_3 -related fluorescence near 6.6 and 8 μm , observed at high pressure by von Rosenberg and Trainor⁹ and attributed by them to electronic and vibrational transitions of electronically excited triplet ozone.

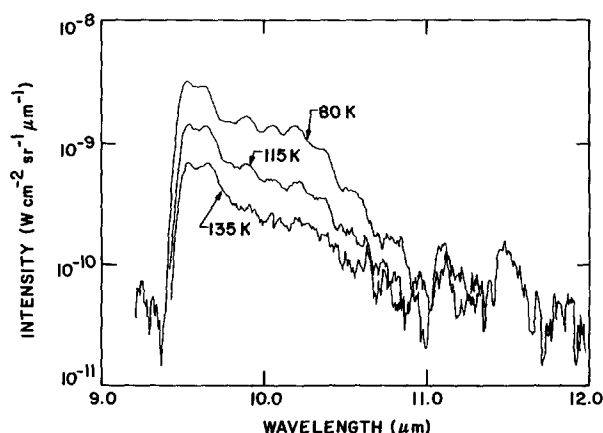


FIG. 2. Effect of temperature, low- O_2 case (no counterflow, 640 $\mu\text{mol/s}$ Ar, 1% O_2 , 0.08 μm resolution).

III. ANALYSIS AND RESULTS

Individual excited state number densities were determined from the spectral data using the linear least-squares spectral fitting method described in paper I.¹⁸ As discussed there, high resolution spectra showed evidence for emission from $(00\nu_3)$ and $[10(\nu_3 - 1)]$ states up to $\nu_3 = 5$, with no observable features from states with $\nu_1 > 1$ or $\nu_2 > 0$. Accordingly, the $(00\nu_3)$ and $[10(\nu_3 - 1)]$ states were included in all the spectral fits. An important aspect of this fitting procedure is that the solutions are values of $N_\nu A_{\nu\nu'}$, where N_ν is the number density for the emitting state and $A_{\nu\nu'}$ is the Einstein coefficient for the radiative transition to the lower state ν' . As discussed in paper I,¹⁸ the scaling of $A_{\nu\nu'}$ with ν' is highly uncertain, and we have chosen a course which could result in underestimates of the values of N_ν . We believe these estimates are reasonably accurate for up to three quanta of stretching excitation, but become progressively more uncertain for the higher levels, with perhaps as much as 50% uncertainty for five quanta. The error bars shown in the following figures reflect only statistical uncertainties from the fitting unless otherwise stated.

An example least-squares fit to spectral data is illustrated in Fig. 3. The slight mismatch between observed and computed rotational distributions, most noticeable in the P/R branch structure of the prominent $(001) \rightarrow (000)$ band near 9.6 μm , appears to be due to a non-Boltzmann rotational distribution resulting from collision-limited $R \leftrightarrow T$ transfer in the low-pressure expansion region of the reaction chamber. However, since the vibrational state number densities are determined from the much coarser band integrals, the results are insensitive to such small discrepancies in the fine structure of the spectrum. Examples of the detailed vibrational state number densities determined from such fits are shown in Fig. 5 of paper I.¹⁸

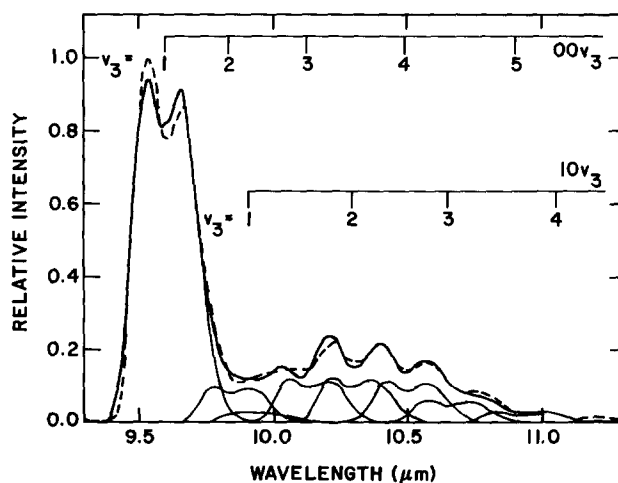


FIG. 3. Comparison of observed and computed (least-squares fit) spectra (11.8% O_2 in Ar, $T = 80$ K, spectral resolution = 0.08 μm ; ---, experimental spectrum; —, computed spectrum and individual vibrational bands, $T_{\text{rot}} = 60$ K).

A. Temperature dependence

The $O_3(v)$ temperature dependence was studied from 80 to 150 K for initial O_2 mole fractions of 0.0067, 0.030, 0.109, and 0.118. In all cases, the individual relative vibrational state populations did not change with temperature, but the total absolute number densities varied by almost an order of magnitude. Accordingly, the total vibrationally excited number densities, $\Sigma_{v>1}[O_3(v)]$, were normalized to a common value at 100 K in order to collapse the data onto a single temperature dependence curve. The results are shown in Fig. 4.

The normalized $\Sigma[O_3(v)]$ values can be fit quite well by a T^{-n} dependence, where $n = (3.2 \pm 0.3)$ at the 95% confidence level. This is considerably larger than $n \approx 2$ as commonly observed for $O + O_2$ recombination with Ar near 300 K.²² However, in Arrhenius form, as plotted in Fig. 5, the COCHISE data extrapolate well to the higher temperature results for the recombination reaction,²⁵⁻²⁸ with approximate asymptotes of $e^{500/T}$ at high T and $e^{250/T}$ at low T . The close correspondence of the temperature dependence of $O_3(v)$ and that of the three-body recombination reaction



is evidence that the $O_3(v)$ observed in COCHISE is formed either directly in reaction (2) or by excitation of ground-state O_3 formed in that reaction.

Since the observed $O_3(v)$ is actually in steady state with collisional deactivation processes, one might expect the temperature dependencies of those processes to influence the behavior of either the relative distributions or the net number densities. The apparent absence of such effects indicates that the overall temperature dependence is controlled by

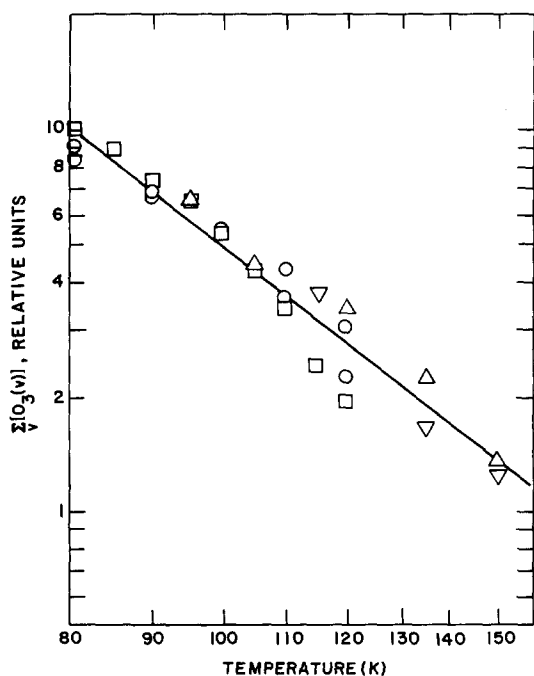


FIG. 4. Temperature dependence of total $[O_3(v)]$ (∇ , 0.67% O_2 ; \circ , 3.0% O_2 ; Δ , 10.9% O_2 ; \square , 11.8% O_2). The solid line is a least-squares fit to the data, $\Sigma_v [O_3(v)] \propto T^{-3.2 \pm 0.3}$ (95% confidence level).

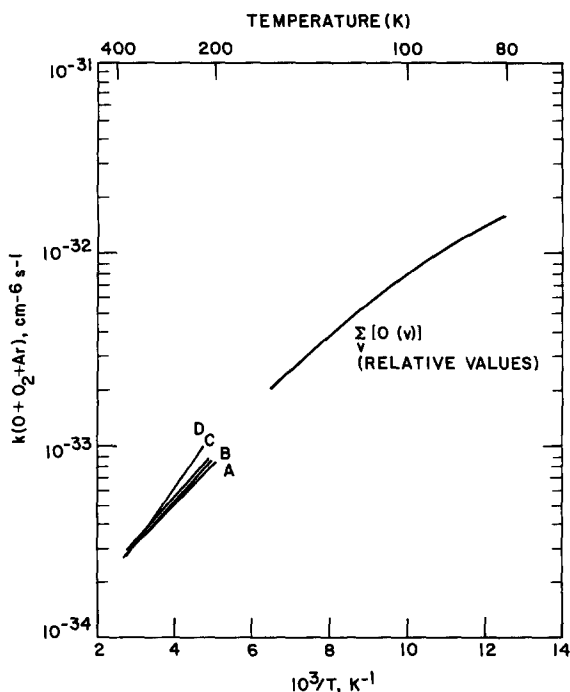


FIG. 5. Arrhenius plot comparing the observed $\Sigma_v [O_3(v)]$ temperature dependence to that observed for the recombination rate coefficient (A: Ref. 25; B: Ref. 26; C: Ref. 27; D: Ref. 28).

that of the O_3 production rate. For $V \rightarrow T$ deactivation processes, viz. $Ar + O_3(v)$, one might expect a weak positive temperature coefficient, perhaps $T^{1/2}$. However, the downward curvature in the data at low T indicates a decreasing $O_3(v)$ production efficiency rather than a decreasing deactivation rate. Thus it appears that the reactions controlling $O_3(v)$ deactivation are not strongly temperature dependent.

B. Variation of O_2 mole fraction

$O_3(v)$ number densities were determined for a variation of χ_{O_2} over slightly more than two orders of magnitude for constant discharge pressure (1.3 Torr) and temperature (80 K). For clarity, we display the results in three figures, Figs. 6 through 8. The overall results, comparing $\Sigma[O_3(v)]$, $[O_3(001)]$, and $\Sigma[O_3(v > 1)]$, are plotted in Fig. 6. Break-

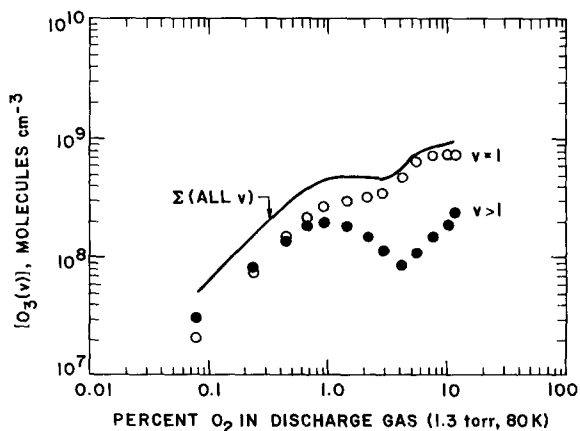


FIG. 6. Observed $O_3(v)$ number densities for all v , $v = 1$, and $v > 1$ (number densities are those observed in the field of view at 3 mTorr).

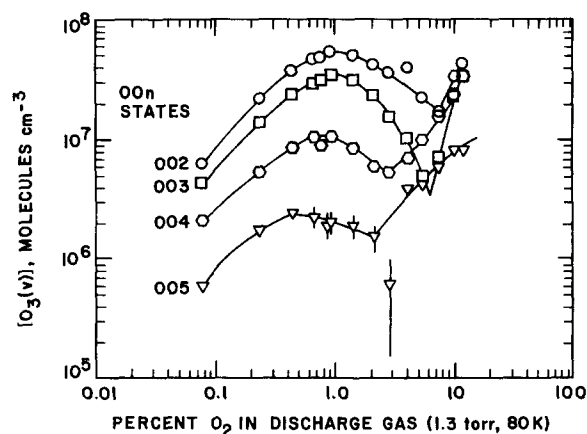


FIG. 7. Observed $O_3(v)$ number densities in field of view, ($00v_3, v_3 > 2$) only.

downs of the individual ($00v_3$) and [$10(v_3 - 1)$] number densities for $v_3 > 1$ are plotted in Figs. 7 and 8, respectively. In general, the data show a roughly first-order dependence on O_2 at low χ_{O_2} , a strong quenching effect for the higher levels above $\chi_{O_2} \sim 0.01$, and a striking increase in $O_3(v)$ production near $\chi_{O_2} \sim 0.1$ which results in population inversions among the higher levels.

The first-order behavior below $\chi_{O_2} = 0.01$ is consistent with our earlier view¹⁷ of $O_3(v)$ formation by reaction (1) balanced by destruction principally by atomic oxygen. The regime above $\chi_{O_2} \sim 0.01$ exhibits a substantial increase in the $O_3(v)$ loss rate, especially for the higher levels; the implication is the onset of another reaction with some discharge-produced species which reaches large concentration at this O_2 level. As we will discuss in the next section, we do not expect O, O_3 , or O_2 to be responsible for this behavior.

The increase in $O_3(v)$ production at large χ_{O_2} seems to originate in the highest observed levels, $v_3 = 4-5$. The production of these levels begins to increase at substantially lower χ_{O_2} than for the lower levels, $v_3 = 2-3$, as if the high levels are directly excited and the lower levels are increasingly populated from above by collisional cascade as χ_{O_2} is increased. Since $O_3(006)$ is not observed even though there is sufficient sensitivity [$[O_3(005)]/[O_3(006)] > 10$], the excitation re-

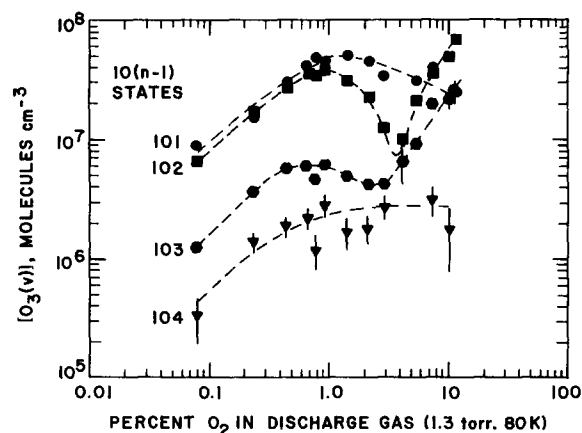
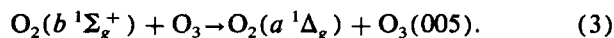


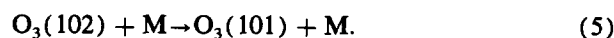
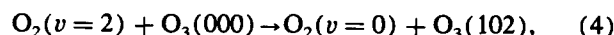
FIG. 8. Observed $O_3(v)$ number densities in field of view [$10(v_3)$ states].

action responsible for these observations must have an energetic limit in the $5000-6000 \text{ cm}^{-1}$ range. Furthermore, since the temperature dependence of $O_3(v)$ tracks with that of recombination even in this regime of χ_{O_2} , the reaction must involve excitation of ground-state O_3 , formed from deactivation of recombination-generated $O_3(v)$. The dramatic increase with χ_{O_2} points to an energetic excitation partner which is formed from electron-irradiated O_2 . The possibilities then are $V \rightarrow V$ transfer to O_3 from $O_2(v)$, or $E \rightarrow V$ transfer from an electronic metastable species. The energy defect we require, ~ 4900 to 5800 cm^{-1} , is significantly off resonance with the states of $O_2(v)$; for example, the $v = 3$ and 4 states of O_2 lie at energies of 4598 and 6085 cm^{-1} , respectively. However, the observed energetics correspond well to the energy difference between $O_2(b^1\Sigma_g^+)$ and $O_2(a^1\Delta_g)$ of 5238.5 cm^{-1} . We therefore invoke the reaction



The quenching of $O_2(b)$ by O_3 has been observed to occur at room temperature with a rate coefficient of $2.2 \times 10^{-11} \text{ cm}^3 \text{ molecule}^{-1} \text{ s}^{-1}$ and a branching fraction of $2/3$ for dissociation of O_3 .²⁹ As will be discussed in the next section, if the remaining $1/3$ of the quenching proceeds by reaction (3), we anticipate that there is sufficient $O_2(b)$ produced in the discharge to account for the observations at large χ_{O_2} .

As discussed in paper I,¹⁸ in the recombination-dominated regime of χ_{O_2} , we observe population of the combination states (103) and (104) in thermal equilibrium with the "pure- v_3 " states (004) and (005), and have interpreted this observation in terms of initial recombination into the v_3 mode followed by rapid, near resonant $V \rightarrow T$ transfer with Ar to populate the nearby [$10(v_3 - 1)$] states. In addition (also in paper I¹⁸), we observe a strong enhancement of [$O_3(102)$] and a minor enhancement of [$O_3(101)$] which is most likely the result of resonant $V \rightarrow V$ exchange with $O_2(v = 2)$:



It is also likely that $O_3(002, 003)$ are enhanced to some extent by deactivation of $O_3(102)$. We have attempted to estimate a lower bound to the total $O_3(v)$ formed from $V \rightarrow V$ exchange by computing from the data the total amount of $O_3(101, 102)$ in excess of the thermal equilibrium with $O_3(002, 003)$ expected for recombination. These values are plotted in Fig. 9. For [$O_3(000)$] estimated by extrapolation of the observed $O_3(v)$ distributions, a value of $\sim 10^{-11} \text{ cm}^3 \text{ s}^{-1}$ for rapid $V \rightarrow V$ exchange, and deactivation by O as described below, the levels of $O_3(v)$ observed in Fig. 9 require an $O_2(v)$ vibrational temperature of $\sim 10^3 \text{ K}$, which is well within the range expected for microwave discharges such as those used here. In addition, the behavior with χ_{O_2} shown in Fig. 9, i.e., a first-order dependence below $\chi_{O_2} = 0.01$ and constant within experimental scatter above that point, has a bearing on the formation kinetics of $O_3(000)$; this point will be addressed in the next section.

We now wish to isolate the effect of recombination kinetics on the vibrational distributions at low χ_{O_2} . In the recombination-dominated regime of χ_{O_2} , we view the observed

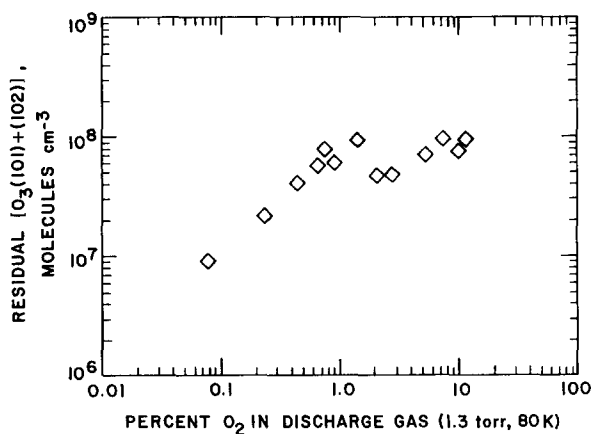


FIG. 9. Estimated contribution from $O_2(v) + O_3$ exchange [number densities (field of view values) represent sum of (102) and (101) values, corrected for their estimated levels due to recombination/deactivation (see the text)].

$O_3(v)$ as being populated by collisional cascade from higher levels which are formed directly in recombination, and destroyed primarily by atomic oxygen. In the steady-state approximation, we have

$$[O_3(v)] = \frac{k_F(v)[O][O_2][Ar]}{k_D(v)[Ar] + k_0(v)[O]} \cong \frac{k_F(v)}{k_0(v)}[O_2][Ar]. \quad (6)$$

As discussed in the next section, the direct formation term $k_F(v)$ does not apply to the relatively low vibrational states observed here, but rather to much higher states which are rapidly deactivated to the lower levels. In this analysis the cascade production rates cannot be treated on a state-to-state basis, so collisional scrambling effects among the lowest five levels are inherent in the values of $k_F(v)$. There is also some contribution from the $V \rightarrow V$ exchange reaction (4), which can be subtracted from the data using the results of Fig. 9. [Note that there is probably some residual contribution from reaction (4) in the (003) and perhaps (002) populations which we cannot evaluate.] Finally, we correct for resonant $V \rightarrow T$ transfer to the combination states by adding the population of each $[10(v_3 - 1)]$ state to that of the corresponding $(00v_3)$ state. A plot of the resulting relative vibrational state populations, $[O_3(00v_3)] / \sum_{v_3 > 1} [O_3(00v_3)]$, as functions of χ_{O_2} is shown in Fig. 10. For $\chi_{O_2} < 0.01$, the data fit well to an exponential empirical expression, with well-defined intercepts at $\chi_{O_2} = 0$. Since $[Ar]$ is constant throughout, the slopes of the lines reflect variations in the atomic oxygen deactivation rates with χ_{O_2} ; variation in the slopes suggests a vibrational level-dependent rate coefficient which increases with v_3 . The intercepts reflect an effective vibrational distribution which is affected only by collisions with argon. A least-squares analysis of the $\chi_{O_2} = 0$ vibrational distribution gives a vibrational "temperature" of $2070 \pm 210(1\sigma)$ K. In the next section, we will attempt to extract from these data further details about the atomic oxygen deactivation and about the nascent or quasi-nascent $O_3(v)$ distribution from three-body recombination.

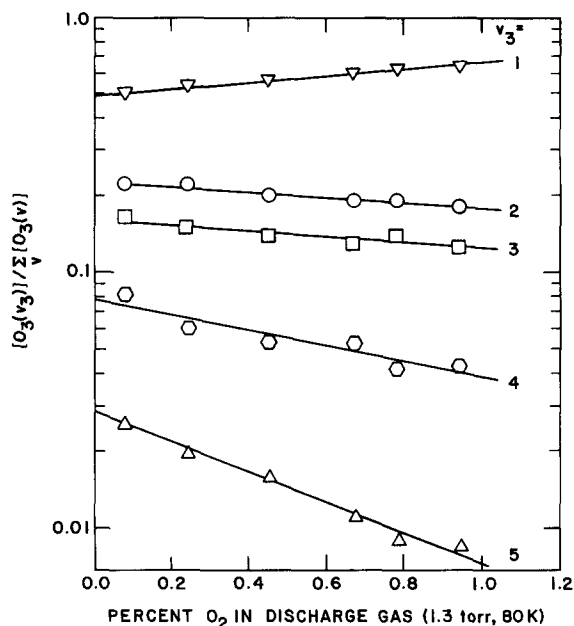


FIG. 10. Dependence of relative vibrational distributions from recombination upon O_2 mole fraction in discharge gas (the solid lines are least-squares fits to the data points).

As a final point in the data analysis, we note the striking difference between the kinetic behavior of $O_3(001)$ and that of the higher levels (cf. Figs. 6 and 10). The relative (001) contribution increases steadily with χ_{O_2} , showing none of the sensitivity to O_2 -related loss processes that are evident in the data for higher v . While a number of hypotheses might account for this, the simplest explanation which satisfies both the reaction order and temperature dependence is that significant $O_3(001)$ might be formed by secondary electron impact excitation of $O_3(000)$, which undoubtedly accumulates in the recombination process. If this is true, then $O_3(001)$ and $O_3(000)$ might well be in a quasiequilibrium, especially at higher χ_{O_2} , where $O_3(000)$ buildup is more substantial. Similar excitation of the higher levels may also occur, however, from inspection of the data, this does not seem to be a dominant contribution.

IV. KINETIC INTERPRETATIONS

In order to fully interpret the data in terms of production and loss mechanisms for $O_3(v)$, we must assess species number densities, rate coefficients, and scalings with χ_{O_2} and T for the relevant reactions which we expect to occur in the microwave discharges. In this section, we first address the physics and chemistry of the discharge in order to estimate number densities of the key species. We then apply these values in a comparative assessment of the various possible $O_3(v)$ production and loss processes. This leads to the derivation of a rigorous steady-state kinetic analysis, which we can then use to interpret the experimental results.

A. Discharge conditions

The COCHISE discharges are of the conventional microwave type, whose operating conditions are governed by ambipolar diffusion.^{30,31} For the conditions of these experi-

ments, we estimate an electric field/density ratio of $E/N \sim 3 \times 10^{-16}$ V cm²; from energy balance considerations, this leads to an estimated electron number density of $\sim 10^{11}$ cm⁻³. We have solved the Boltzmann transport equation, treating all the inelastic processes occurring in the discharge to the accuracy with which their cross sections are known, to obtain a characteristic electron energy of ~ 8 eV for dilute O₂/Ar mixtures. This characteristic energy is roughly constant from $\chi_{O_2} = 0$ to 0.01, and then decreases with increasing χ_{O_2} due to increasing collision frequency of electrons with O₂, approaching a value of ~ 2 eV for 100% O₂. Application of the electron energy distributions obtained in this fashion to energy-dependent excitation cross sections available in the literature gives the effective excitation rate coefficients as functions of E/N and χ_{O_2} .

We have used this treatment to estimate rate coefficients for the key electron impact processes, including O₂ dissociation (O formation), excitation of O₂(ν) and of the O₂ metastables $a^1\Delta_g$, $b^1\Sigma_g^+$, $c^1\Sigma_u^-$, and dissociation of O₃ (a key O₃ loss process). An important aspect of these calculations is that, since the electron energy distribution is unaffected by O₂ at low χ_{O_2} , the excitation rate coefficients are constant below $\chi_{O_2} = 0.01$, i.e., in the recombination-dominated regime. This means that the production rates for O, O₂(ν), and O₂(a, b, c) are linearly dependent upon [O₂] in this regime. We will use these rate coefficients in the steady-state analysis presented below. Further details on the Boltzmann transport solutions are given in the Appendix.

B. Excitation of O₃(ν)

We wish to evaluate and compare the O₃(ν) production rates for the most likely reactions: three-body recombination; electron-impact excitation, resonant V→V transfer from O₂($\nu = 2$); resonant E→V transfer from O₂($b^1\Sigma_g^+$); and the possible chemical reaction between O₂ and one or more of the high-lying metastables O₂($A^3\Sigma_u^+$, $A'^3\Delta_u$, $c^1\Sigma_u^-$). The reactions considered are listed in Table I, along with their estimated rates for $\chi_{O_2} = 10^{-3}$, 10^{-2} , and 10^{-1} .

To estimate the three-body recombination rate, we use values of [O] given by the discharge analysis. O is formed by electron-impact dissociation of O₂, and its number density is limited by the residence time t in the discharge. Thus we

have $[O]/[O_2] = 2k_E^{O_2}[e^-]/t$. For $k_E^{O_2}$ as determined for the COCHISE discharges, we get $[O]/[O_2] \sim 1$ for $\chi_{O_2} \leq 10^{-2}$ and $[O]/[O_2] \sim 0.2$ for $\chi_{O_2} = 10^{-1}$. From Fig. 5, we estimate a recombination rate coefficient of $k_R \sim 2 \times 10^{-32}$ cm⁶ s⁻¹ at 80 K; this then gives a product $k_R [O][O_2][Ar] = 2 \times 10^{13}$, 2×10^{15} , and 4×10^{16} cm⁻³ s⁻¹ for $\chi_{O_2} = 10^{-3}$, 10^{-2} , and 10^{-1} , respectively.

The next three reactions in Table I involve excitation by energy transfer to O₃(000), whose number density must be estimated from the discharge calculations. The only efficient means of forming O₃(000) in the discharge is by the recombination/vibrational relaxation pathway; the above total O₃(ν) production rates provide an upper bound for O₃(000) formation. The principal loss process for O₃(000) is most likely by electron-impact dissociation; we estimate a loss rate on the order of 10^3 s⁻¹ based on the discharge predictions. Dissociation of O₃ by metastables of O, O₂, or Ar proves to be more than an order of magnitude slower by comparison. Thus we estimate upper-bound values for [O₃(000)] of 2×10^{10} , 2×10^{12} , and 4×10^{13} cm⁻³ for $\chi_{O_2} = 10^{-3}$, 10^{-2} , and 10^{-1} . The value at $\chi_{O_2} = 10^{-2}$ is consistent with extrapolation of the observed vibrational distribution and correction for the expansion pressure ratio, i.e., [O₃(000)]/[O₃(001)] ~ 25 . The actual [O₃(000)] value may be considerably less than this owing to incomplete vibrational relaxation.

Vibrational excitation of O₃ by low-energy electrons is difficult to assess since its cross section is unknown and the effective electron density is ill defined. If we describe the process in terms of the total electron density and an effective rate coefficient of 10^{-9} cm³ s⁻¹, the upper-bound excitation rates are about an order of magnitude smaller than those for recombination. Thus this reaction may compete with recombination for formation of O₃(001), but does not appear to be effective for general excitation of O₃(ν).

O₂(ν) is formed in the active discharge by electron-impact excitation of O₂, and is removed by deactivation by O and electron-impact dissociation. For low vibrational levels, the O-atom reaction is the dominant loss process by one to two orders of magnitude. From the discharge predictions and a likely O + O₂(ν) rate coefficient of $\sim 10^{-11}$ cm³ s⁻¹, we expect [O₂($\nu = 2$)] = 8×10^{12} , 8×10^{12} , and 4×10^{13} cm⁻³ at $\chi_{O_2} = 10^{-3}$, 10^{-2} , and 10^{-1} , corresponding to vibrational "temperatures" of about 1700, 900, and 800 K, respectively. The actual temperatures could be significantly higher due to V↔V self-pumping by O₂, not considered here. For an O₂-O₃ V→V transfer rate coefficient of $\sim 10^{-11}$ cm³ s⁻¹, we obtain O₃(102) production rates which are competitive with those expected for recombination. The values listed in Table I are also consistent within a factor of 2 with the apparent O₃(102) production rate determined from the data of Fig. 9 using the deactivation rates derived below. The O₂(ν) + O₃ hypothesis therefore appears to be quite credible in terms of both the data and the expected discharge kinetics.

O₂($b^1\Sigma_g^+$) is formed and dissociated by electron impact. The dissociation cross section is not known, but the effective rate coefficient can be scaled from the O₃(ν) data. From the onset of the O₃(ν) enhancements shown in Fig. 7,

TABLE I. Estimated rates^a of O₃(ν) formation in microwave discharges of O₂/Ar, 1.3 Torr, 80 K.

Reaction	$\chi_{O_2} = 10^{-3}$	10^{-2}	10^{-1}
O + O ₂ + Ar → O ₃ (ν) + Ar	2 (13) ^b	2 (15)	4 (16)
e + O ₃ → O ₃ (001) + e ⁻	<2 (12)	<2 (14)	<4 (16)
O ₂ ($\nu = 2$) + O ₃ → O ₃ (102) + O ₂	2 (12)	2 (14)	2 (16)
O ₂ ($b^1\Sigma$) + O ₃ → O ₃ (005) + O ₂	1 (11)	1 (14)	6 (15)
O ₂ ($c^1\Sigma$) + O ₂ → O ₃ (001,002) + O	...	1-10 (13)	...

^aRates are in units of molecules cm⁻³ s⁻¹.

^b2 (13) represents 2×10^{13} .

together with an $E \rightarrow V$ rate coefficient of $7 \times 10^{-12} \text{ cm}^3 \text{ s}^{-1}$ (in keeping with the results of Slanger and Black²⁹), we estimate $[\text{O}_2(b)]$ values which, taken with the discharge-predicted $\text{O}_2(b)$ production rates, correspond to an $\text{O}_2(b)$ dissociation rate coefficient which is about five times larger than that for $\text{O}_2(X^3\Sigma_g^-)$. This gives $[\text{O}_2(b)] = 10^{12}, 10^{13}$, and $2 \times 10^{13} \text{ cm}^{-3}$ for $\chi_{\text{O}_2} = 10^{-3}, 10^{-2}$, and 10^{-1} . The resulting $\text{O}_3(005)$ production rates, shown in Table I, are seen to be competitive with recombination only at large χ_{O_2} .

Lastly, we consider the reaction



where O_2^* is one of the Herzberg states: $A^3\Sigma_u^+$, $A'^3\Delta_u$, and $c^1\Sigma_u^-$. This type of reaction was implicated in high altitude auroral measurements,^{19,21} but has yet to be demonstrated in the laboratory. The reaction with $\text{O}_2(A, v=0)$ is exoergic enough to form O_3 with up to two quanta of stretching vibration. For $\chi_{\text{O}_2} = 10^{-2}$, we estimate from the discharge predictions for $\text{O}_2(c)$ an O_2^* production rate of $\sim 6 \times 10^{16} \text{ cm}^{-3} \text{ s}^{-1}$. By analogy with the other metastables, the loss rate by dissociation is probably 10^4 – 10^5 s^{-1} , so we expect $[\text{O}_2^*] = \sim 10^{11}$ – 10^{12} cm^{-3} . This means that reaction (7) may compete successfully with recombination if the rate coefficient is in the $10^{-13} \text{ cm}^3 \text{ s}^{-1}$ range, a value which is consistent with quenching measurements at room temperature for $\text{O}_2(A)$.³² However, the strong negative temperature coefficient observed for all $\text{O}_3(v)$ under all χ_{O_2} conditions argues against the contribution of reaction (7) in the COCHISE measurements at cryogenic temperatures.

C. Deactivation of $\text{O}_3(v)$

The principal loss of $\text{O}_3(v)$ occurs through collisions with Ar, the wall of the discharge tube, and atomic oxygen. Deactivation by O_2 is not important at these dilutions. In addition, we will consider dissociation of $\text{O}_3(v)$ by electrons, $\text{O}_2(a^1\Delta_g)$, and $\text{O}_2(b^1\Sigma_g^+)$. The relevant reactions are listed in Table II.

The deactivation of low levels of $\text{O}_3(v)$ by Ar has been studied at room temperature.^{2-4,12} We have scaled those data by $vT^{1/2}$ to apply to our conditions. Based on the state distri-

butions we observe, it appears that the deactivation occurs mainly by $\Delta v_3 = 1$ changes until the (001) state is reached, after which it may proceed through (010) into (000) as suggested by Rosen and Cool.^{2,3} For this type of $V \rightarrow T$ transfer, we expect single quantum cascade down the vibrational ladder. The assumed Ar deactivation rates are therefore in the 10^3 s^{-1} range, with a significant dependence on vibrational level.

Deactivation of $\text{O}_3(v)$ on the wall of the discharge tube was estimated from lowest mode diffusion³⁰ by analogy to CO_2 ,^{17,33} assuming unit deactivation efficiency. This gives an upper bound of $\sim 300 \text{ s}^{-1}$, which is of minor importance for our conditions. This value is comparable to 500 s^{-1} corresponding to the inverse of the residence time in the active discharge prior to expansion, so little influence of wall collisions on the vibrational distributions is expected.

Deactivation of $\text{O}_3(v)$ by O is a critical reaction which is difficult to treat. West *et al.*⁵ studied this reaction for $\text{O}_3(v=1)$ and found efficient removal of $\text{O}_3(v)$ by O, with a rate coefficient of either $\sim 10^{-11}$ or $\sim 10^{-12} \text{ cm}^3 \text{ s}^{-1}$, depending upon whether chemical reaction or $V \rightarrow T$ transfer occurred. These same investigators⁶ later reported no significant loss of O in the process, implicating $V \rightarrow T$ transfer as the dominant pathway, at least for $\text{O}_3(v=1)$. The behavior for higher v is not known, although statistical arguments³⁴ favor deactivation by multiquantum energy transfer. For reasons discussed later in this paper, we suspect that the chemical reaction pathway plays a role in our experiments. For the present purposes, we invoke a rate coefficient of $10^{-11} \text{ cm}^3 \text{ s}^{-1}$ with no dependence upon vibrational level. For this value, we can see that deactivation by O is competitive with Ar at the lowest χ_{O_2} and faster for larger χ_{O_2} . In the analysis to follow, we will use the data to obtain better estimates for the rate of this process.

The rate of dissociation of $\text{O}_3(v)$ by electrons was estimated by analogy with $\text{O}_3(000) + e^-$ rates determined above, assuming no large increase in the rate with O_3 vibrational energy. This loss process may be a minor factor at low χ_{O_2} , but does not appear to be generally important except to determine the overall loss rate of total ozone.

The dissociation of $\text{O}_3(v)$ by $\text{O}_2(a^1\Delta_g)$ is an interesting possibility and may provide an explanation for the anomalously large loss rates for $\text{O}_3(v \geq 2)$ which are evident in the data (Figs. 6 through 8) for $\chi_{\text{O}_2} > 10^{-2}$. Quenching of vibrationally cold $\text{O}_2(a)$ by ground state O_3 is known to be slow²²; however, excitation of at least one vibrational quantum of either partner would permit dissociation of the O_3 , and might therefore lead to a substantial increase in the reaction cross section. Based on the discharge predictions, we estimate $[\text{O}_2(a)] \sim 10^{14}$ to $4 \times 10^{15} \text{ cm}^{-3}$ for $\chi_{\text{O}_2} = 10^{-2}$ to 10^{-1} . Thus we can account for the observations with a rate coefficient in the 10^{-11} to $10^{-10} \text{ cm}^3 \text{ s}^{-1}$ range. We know of no other possible hypotheses to explain the observed depletion in $\text{O}_3(v \geq 2)$ above $\chi_{\text{O}_2} = 10^{-2}$.

Finally, we have evaluated the dissociation of $\text{O}_3(v)$ by $\text{O}_2(b^1\Sigma_g^+)$ using the discharge predictions given above for $[\text{O}_2(b)]$ and the total quenching constant of Slanger and Black²⁹ for ground-state O_3 . As shown in Table II, this turns out to be an insignificant loss process for $\text{O}_3(v)$.

TABLE II. Estimated loss rates^a for $\text{O}_3(v)$ in microwave discharges of O_2/Ar , 1.3 Torr, 80 K.

Reaction	$\chi_{\text{O}_2} = 10^{-3}$	10^{-2}	10^{-1}
$\text{O}_3(v) + \text{Ar}$ $\rightarrow \text{O}_3(v-1) + \text{Ar}$	$700v$	$700v$	$700v$
$\text{O}_3(v) \xrightarrow{\text{wall}} \text{O}_3(v-n)$	< 300	< 300	< 300
$\text{O}_3(v) + \text{O}$ $\rightarrow 2\text{O}_2$	1 (3) ^b	1 (4)	2 (4)
or $\text{O}_3(v-n) + \text{O}$			
$\text{O}_3(v) + e^-$ $\rightarrow \text{O}_2 + \text{O}$	1 (3)	1 (3)	1 (3)
$\text{O}_3(v) + \text{O}_2(a^1\Delta)$ $\rightarrow 2\text{O}_2 + \text{O}$	1–10 (2)	1–10 (3)	4–40 (4)
$\text{O}_3(v) + \text{O}_2(b^1\Sigma)$ $\rightarrow 2\text{O}_2 + \text{O}$...	1 (2)	...

^a Rates are in units of molecules s^{-1} .

^b 1 (3) represents 1×10^3 .

D. Steady-state kinetic analysis

Comparison of the estimated $O_3(v)$ production and loss rates in Tables I and II allows us to confidently verify our initial belief that, for $\chi_{O_2} < 10^{-2}$, $O_3(v)$ is formed primarily through three-body recombination and is removed by collisions with O and Ar. The values of Tables I and II give predicted steady-state $O_3(v)$ number densities in the field of view of $\sim 3 \times 10^7$, 7×10^8 , and $3 \times 10^9 \text{ cm}^{-3}$ for $\chi_{O_2} = 0.001$, 0.01, and 0.1, respectively. The first two values are within a factor of ~ 2 of the observations (cf. Fig. 6), which is well within the uncertainty of the calculations. The predicted value at $\chi_{O_2} = 0.1$ is high by a factor of ~ 3 , suggesting that we may have underestimated some of the loss rates for this discharge condition.

The excited ozone observed in these experiments is in low vibrational states, $v < 5$, which are unlikely to have been formed directly upon stabilization of the $O_2\text{-O}$ collision complex. We define here a true nascent distribution, $O_3(v^*, J^*)$, as being the earliest rotational-vibrational distribution for which collisional redissociation is insignificant compared to radiative and/or collisional deactivation. This distribution is likely to encompass vibrational states in the upper third or half of the potential well, and is also probably extremely short lived, perhaps surviving for only 100 collisions. On this time scale there will evolve a secondary vibrational distribution, $O_3(v)$, which is the quasiinitial distribution that precedes the deactivation observed here. The states within this distribution are populated by downward collisional cascade, not by direct recombination. Thus for each state there are several production terms involving higher-lying states, which in turn have more production terms. For algebraic simplicity, we treat the $O_3(v)$ states collectively, such that collisional "scrambling" among the individual states is an inherent part of the distribution. In terms of the steady-state analysis for collective $[O_3(v)]$, it is easy to show that a steady-state assumption of $O_3(v^*, J^*)$ formation by three-body recombination and removal by Ar gives the same form for the production rate for $O_3(v)$ as if we assume direct recombination into $O_3(v)$. We can therefore write the level-dependent steady-state equations [cf. Eq. (6)]:

$$[O_3(v)] = \frac{k_v^R [O][O_2][Ar]}{k_v^O [O] + R_v}, \quad (8)$$

$$\sum_v [O_3(v)] = \frac{\sum_v k_v^R [O][O_2][Ar]}{k_L^O [O] + R_1}, \quad (9)$$

where k_v^R is the apparent rate coefficient for "direct" recombination into state v , k_v^O is the rate coefficient for collisional removal of state v by O, and R_v represents the removal of state v by all oxygen-independent processes, mainly Ar and wall collisions. In Eq. (9), k_L^O represents the rate-limiting step for removal of all $O_3(v)$ by O. For example, if the $O + O_3(v)$ step proceeds by single quantum cascade, this is given by $k_L^O = k_1^O$; if the process is a chemical reaction or involves total multiquantum deactivation to $O_3(v=0)$, we have $k_L^O = \sum_v k_v^O [O_3(v)] / \sum [O_3(v)]$.

Several important conclusions can now be stated upon examination of the reaction orders observed in Figs. 6 through 8. First, the observed number densities of $\sum [O_3(v)]$

(v) and $[O_3(v)]$ are first order in O_2 even at the lowest χ_{O_2} , corresponding to $[O_2] = 1.3 \times 10^{14} \text{ cm}^{-3}$. From the discharge predictions, we expect $[O]/[O_2]$ to be constant throughout this regime, with an estimated ratio of unity. From the condition required for first-order behavior, $k_v^O [O] > R_v$ and R_v given by Table II, we conclude $k_1^O > 8 \times 10^{-12} \text{ cm}^3 \text{ s}^{-1}$, etc., up to $k_5^O > 3 \times 10^{-11} \text{ cm}^3 \text{ s}^{-1}$. Further information on the deactivation step can be gleaned from the $V \rightarrow V$ transfer results plotted in Fig. 9. From the discharge predictions, we expect $(O_2(v=2))$ to be constant from $\chi_{O_2} = 10^{-3}$ to 10^{-2} . The first-order behavior in $[O_3(102)]$ exhibited in Fig. 9 must therefore be due to a similar dependence in $[O_3(v=0)]$. First-order behavior of $[O_3(v=0)]$ cannot occur if there is significant formation of $O_3(v=0)$ by $O + O_3(v)$. This, together with the large values of k_v^O , indicates that the major route of the $O + O_3(v)$ step is chemical reaction to form O_2 .

To assess the level-dependent kinetic effects, we examine the relative vibrational distributions

$$\frac{[O_3(v)]}{\sum_v [O_3(v)]} = \frac{k_v^R k_L^O [O] + R_1}{\sum_v k_v^R k_v^O [O] + R_v}. \quad (10)$$

It can be shown after considerable algebra that, over the range of $[O]$ and relative population observed here, Eq. (10) is approximated by the empirical exponential form plotted in Fig. 10. The empirical slopes are related to the kinetic parameters via

$$\frac{d \ln \{ [O_3(v)] / \sum_v [O_3(v)] \}}{d [O_2]} \cong \frac{f k_L^O}{R_1} - \frac{f k_v^O}{R_v} \quad (11)$$

to within $\sim 30\%$, where $f = [O]/[O_2] \approx 1$. The first-order kinetics in $[O_2]$ provides us with the lower bound $k_L^O/R_1 > 8 \times 10^{-15} \text{ cm}^3$. Using the Ar and wall deactivation rate coefficients from Table II, and the empirical slopes from Fig. 10, we can evaluate lower bounds for k_v^O : (0.8, 1.4, 2.0, 2.7, and $3.6) \times 10^{-11} \text{ cm}^3 \text{ s}^{-1}$ for $v = 1, 2, 3, 4$, and 5, respectively.

The $\chi_{O_2} = 0$ intercepts from Fig. 10 can be used to determine the quasiinitial $O_3(v)$ distribution from recombination. From Eq. (10) at $[O] = 0$, we obtain

$$\left(\frac{[O_3(v)]}{\sum_v [O_3(v)]} \right) = \frac{k_v^R R_1}{\sum_v k_v^R R_v}, \quad (12)$$

where $k_v^R / \sum_v k_v^R$ are the quantities we seek. The observed intercepts and the values corrected for R_v/R_1 are plotted in Fig. 11. The error bars reflect the combined uncertainties in R_v/R_1 (i.e., with and without wall collisions) and in the Einstein coefficients used in the spectral analysis. Also plotted in Fig. 11 is the statistical nascent distribution which would obtain if the entropy change of the reaction were maximized, i.e., if all final states within the v_3 mode were equally probable. In the language of surprisal theory,³⁵ this is called the "prior" or "zero surprisal" distribution of states, and is given by³⁶

$$P^0(v) = \frac{(1 - E_v/E)^{3/2}}{\sum_v (1 - E_v/E)^{3/2}}, \quad (13)$$

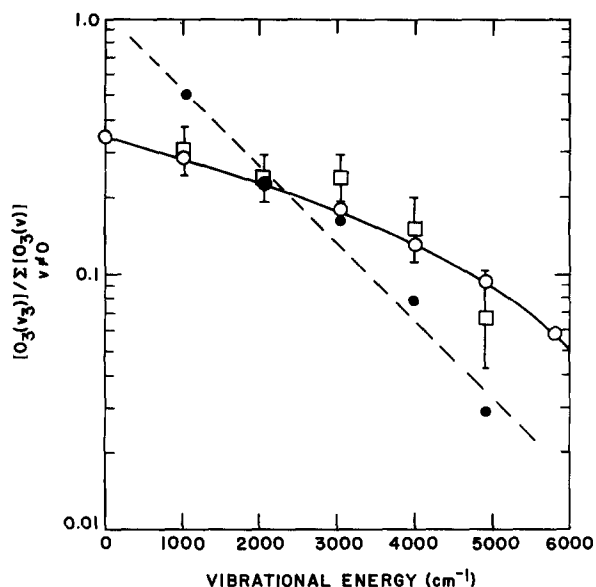


FIG. 11. Quasiinitial vibrational distribution of $O_3(v)$ formed in recombination [---●---, $\chi_{O_2} = 0$ intercepts, with least squares-fit [$T_{vib} = 2070 \pm 210(1\sigma)$ K]; □, zero- O_2 values adjusted for Ar deactivation; -○-, computed statistical distribution (including $v = 0$)].

where E_v is the energy of vibrational state v and E is the total energy available ($E = 8468 \pm 140 \text{ cm}^{-1}$). The close correspondence between the COCHISE quasiinitial distribution and the zero surprisal distribution is striking. It appears from this that the energy contained in the truly nascent $O_3(v^*, J^*)$ states is rapidly randomized throughout the asymmetric stretching mode of the molecule in collisions with the Ar bath gas.

V. DISCUSSION

The detailed dynamics of three-body recombination are summarized in Table III. In the energy transfer or association/deactivation mechanism, we envision the formation of an unbound but associated $O\cdots O_2$ complex which can live long enough to collide with an Ar atom. This collision results in either dissociation of the complex or formation of slightly bound $O_3(^*)$. Further collisions of $O_3(^*)$ result in either

TABLE III. Dynamics of three-body recombination.

(1) Association/deactivation mechanism	
Complex formation:	$O + O_2 \rightarrow O\cdots O_2 \rightarrow O + O_2$ $O\cdots O_2 + M \rightarrow O + O_2 + M$ $O\cdots O_2 + M \rightarrow O_3(^*) + M$
Stabilization:	$O_3(^*) + M \rightarrow \rightarrow O + O_2 + M$ $O_3(^*) + M \rightarrow \rightarrow O_3(v^*, J^*) + M$
Deactivation	$O_3(v^*, J^*) + M \rightarrow \rightarrow O_3(v) + M$ $O_3(v) + M \rightarrow \rightarrow$ Rotational thermalization Vibrational cascade
(2) Chaperon mechanism	
	$O + M \rightleftharpoons OM$ $O_2 + OM \rightarrow O_2 + O + M$ $O_2 + OM \rightarrow O_3(v^*, J^*) + M$ $O_3(v^*, J^*) + M \rightarrow \rightarrow$ Rotational thermalization Vibrational cascade

redissociation or stepwise deactivation until finally the non-dissociative nascent distribution $O_3(v^*, J^*)$ is attained. The state distribution continues to evolve downwards by collisional cascade, at first rapidly through V,R \rightarrow T transfer until the rotational distribution is thermalized, and then more slowly by conventional V \rightarrow T transfer thereafter. Within the framework of this model, we require rapid scrambling of the recombination energy throughout the v_3 mode. This is not unreasonable, since trajectory calculations for $Ar + O_3(v, J)$ collisions indicate efficient energy transfer with large ΔE for excited ozone molecules with high rotational energy.^{37,38} The observed preference for asymmetric stretching motion is also striking; it seems that the newly formed molecules (probably in a quasicontinuum of states) are deactivated into the nonchaotic portion of the potential well so rapidly that they retain "memory" of the original approach configuration. The decrease in the recombination rate with increasing temperature can be ascribed, qualitatively at least, to less efficient complex formation and increased collisional redissociation prior to formation of the nascent distribution.

In an alternative recombination scheme, the chaperon or radical-molecule complex mechanism, O and Ar may exist in equilibrium with the weakly bound van der Waals molecule ArO , which can react with O_2 to either dissociate or form excited O_3 . Troe³⁹ has suggested that this mechanism may be responsible for the anomalously low values for the three-body and high-pressure rate coefficients observed for the reaction at room temperature. We can find no evidence in our data to preclude the occurrence of this mechanism. A detailed study of these mechanisms using classical trajectory calculations is currently under way in our laboratory; preliminary results indicate an $O_3(v)$ production rate by the chaperon mechanism which is much smaller than that obtained from Fig. 5.⁴⁰

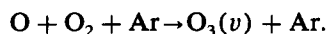
The elusive triplet excited state of ozone^{41,42} may also be involved in the recombination sequence, perhaps as a collisional precursor to the quasiinitial $O_3(v)$ distribution. Our data neither support nor contradict this, however, there is no spectral evidence for significant triplet ozone,¹⁸ nor do we need to invoke its presence to account for the results.

The COCHISE data have profound significance in the interpretation and modeling of high-altitude $O_3(v)$ chemistry.¹⁹⁻²¹ We expect the observed quasiinitial distribution to correspond fairly well to the three-body recombination reaction in the upper atmosphere. The effects of N_2 and O_2 as third bodies and V \rightarrow T collisional deactivation partners should be similar to those observed here for Ar. Furthermore, the large rate coefficients we find for reaction of $O_3(v)$ with O indicate that the atomic oxygen reaction will be important between 80 and 100 km for some (but not all) atmospheric conditions. Finally, the characterization of other discharge-related $O_3(v)$ excitation processes has an important bearing on the interpretation and scaling of auroral observations.

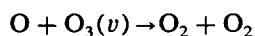
VI. CONCLUSIONS

By a detailed analysis of spectrally resolved $O_3(v)$ fluorescence data over a wide range of experimental conditions,

we have been able to characterize completely the kinetics of $O_3(v)$ formed in microwave discharges of dilute, flowing O_2/Ar mixtures. The primary result of this effort is the determination of the quasiinitial distribution of $O_3(v)$ states formed in three-body recombination of O with O_2 ,

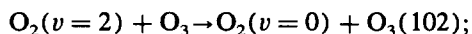


The results indicate statistical behavior in the asymmetric stretch mode, but little or no transfer into the other modes on the time scale of the measurements. An analysis of the change in vibrational distribution with changing O_2 mole fraction leads to the conclusion that deactivation of $O_3(v)$ by O proceeds via chemical reaction:

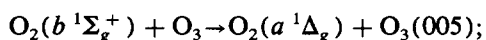


with rate coefficients in excess of $10^{-11} \text{ cm}^3 \text{ s}^{-1}$ and increasing with v . As an interesting aside, this reaction can lead to considerable vibrational and electronic excitation in O_2 , including the formation of the metastables $A^3\Sigma_u^+$, $A'^3\Delta_u$, and $c^1\Sigma_u^-$.

Additional evidence was obtained for other $O_3(v)$ excitation processes. These include: resonant V→V transfer from $O_2(v)$,



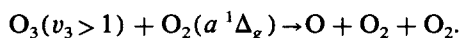
resonant E→V transfer from $O_2(b^1\Sigma_g^-)$,



and possibly electron-impact excitation of O_3 ,



Finally, indirect evidence suggests rapid dissociation of $O_3(v_3 > 1)$ by $O_2(a^1\Delta_g)$:



Much of the information presented here was inferred from indirect and often circuitous analysis of a complex data base. For this reason, these results are by no means definitive. Nevertheless, they represent the current state of the art for this difficult problem, and the development of a more definitive data base will undoubtedly prove to be extraordinarily difficult. We eagerly await the testing of the concepts and models presented here by advanced theoretical and experimental methods.

ACKNOWLEDGMENTS

The authors thank B. D. Green and A. Gelb for many stimulating discussions, H. C. Murphy for assistance with the experiments, and L. M. Cowles and J. F. Cronin for portions of the data analysis. This research was supported by the Defense Nuclear Agency and the Air Force Office of Scientific Research.

APPENDIX: THE PREDICTION OF EXCITATION RATE CONSTANTS IN O_2/Ar DISCHARGES

We present here predictions for excitation rates in O_2/Ar microwave discharges. These calculations not only incorporate the collective effects of ground-state excitation of O_2 but also include excitation of discharge created species such as cross sections for O-atom excitation, ozone dissocia-

tion, and ionization of argon metastable states.

We have used a computer model which solves the Boltzmann transport equation to evaluate the excitation rates characteristic of the O_2/Ar discharges used in the COCHISE ozone studies. Discharge predictions were performed for various O_2/Ar mixtures as a function of E/N (electric field per unit length normalized by total number density). The inputs to these calculations are the electron energy dependent cross sections for the inelastic processes occurring in the discharge while the outputs include discharge characteristics such as characteristic electron energy and drift velocity as well as excitation rate constants. The calculational techniques are straightforward and well understood (see, e.g., Ref. 43).

The predictions are, of course, only as accurate as the cross sections employed. In the case of argon all the cross sections are well known with the exception of those for electronic excitation. We have characterized electronic excitation with two processes representing s state excitation with an energy loss of 11.6 eV and p state excitation with an energy loss of 13.1 eV. These cross sections were used with the more standardly accepted cross sections for momentum transfer and ionization for $Ar^{43,44}$ to predict the transport properties of argon discharges. Predicted values of drift velocity, characteristic energy, and ionization coefficient as functions of E/N gave good agreement with experimental measurements for argon discharges.

For the case of O_2 the cross section data base discussed extensively by Phelps and co-workers⁴⁶⁻⁴⁸ has been used. These cross sections provided reasonable agreement with O_2 discharge data and limited measurements of O_2 metastable state excitation rates.^{46,47} The processes considered include momentum transfer, rotational and vibrational excitation, electronic excitation of several states, dissociation, dissociative attachment, and ionization.

Several excitation processes involving O and O_3 have also been included in the analysis. These species have been treated as traces and thus do not affect the discharge electron energy distribution. Electron-impact excitation of $O(^3P)$ to $O(^1D)$ and $O(^1S)$ has been specified by the cross sections recommended by Jackman *et al.*,⁴⁹ and dissociation of O_3 by the analysis of Keto.⁵⁰ The latter treatment is theoretical with no experimental validation.

Similarly, electron-impact ionization of the $Ar(4s, 4p)$ states has also been incorporated. These cross sections have been taken from the theoretical treatment in Ref. 51. The cross sections for $Ar(4s)$ have been validated experimentally. Ar metastables were only treated as a trace in the calculations. Note, however, that this stepwise ionization process can change the discharge operating conditions if the Ar metastable state concentration becomes sufficiently large.

These cross sections have been used to calculate discharge properties and excitation/deexcitation rate coefficients of various O_2/Ar mixtures as a function of E/N . Some of the predictions are shown in Figs. 12 through 16. These rate coefficients were used in the kinetic analysis presented in Sec. IV. More detailed tabulations and plots of the relevant cross section data and predicted rate coefficients are available from the authors upon request.

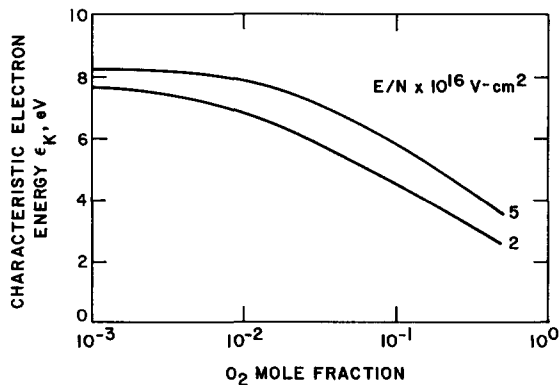


FIG. 12. Predicted characteristic energies in microwave excited mixtures of O_2/Ar .

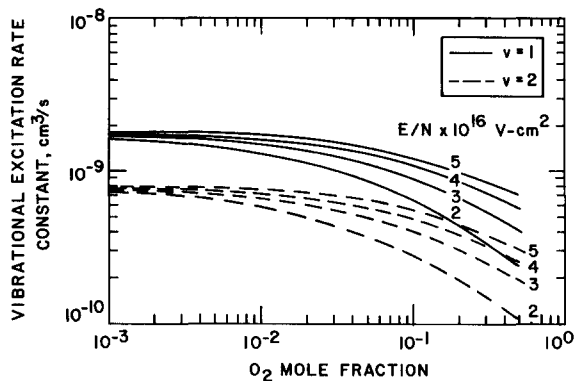


FIG. 15. Predicted rate constants for direct excitation of vibrational levels $v = 1$ and 2 of O_2 in microwave excited mixtures of O_2/Ar .

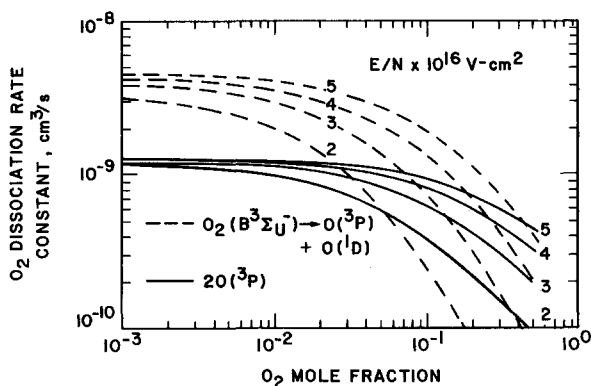


FIG. 13. Predicted rate constants for O_2 dissociation in microwave excited O_2/Ar discharges.

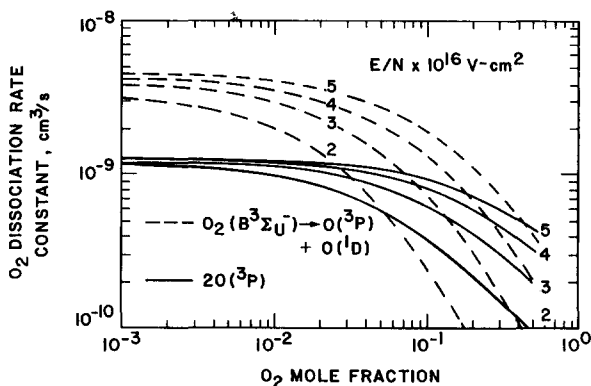


FIG. 16. Predicted rate constants for electron-impact dissociation of O_3 in microwave excited O_2/Ar mixtures.

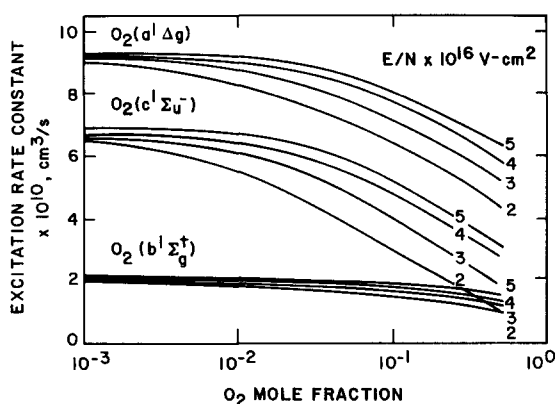


FIG. 14. Rate constants for electron-impact excitation of ground state O_2 to several metastable states for microwave excited O_2/Ar mixtures.

It must be noted that these predictions should not be considered to be exact. Indeed, at these high characteristic energies the adequacy of the first-order expansion of the transport equation is in question. In addition, superelastic collisions have not been accounted for and it has been assumed that the O and O_3 concentrations are traces relative to those for O_2 . If the latter assumption is valid, and given

the accuracy of the cross sections, we expect the rate constants to be accurate to within a factor of 2. Furthermore, at very high excitation levels additional processes should be considered, e.g., electron-impact dissociation of the metastable states of O_2 .

- ¹J. Troe, *Annu. Rev. Phys. Chem.* **29**, 223 (1978).
- ²D. I. Rosen and T. A. Cool, *J. Chem. Phys.* **59**, 6097 (1973).
- ³D. I. Rosen and T. A. Cool, *J. Chem. Phys.* **62**, 466 (1975).
- ⁴K. K. Hui, D. I. Rosen, and T. A. Cool, *Chem. Phys. Lett.* **32**, 141 (1975).
- ⁵G. A. West, R. E. Weston, Jr., and G. W. Flynn, *Chem. Phys. Lett.* **42**, 488 (1976).
- ⁶G. A. West, R. E. Weston, Jr., and G. W. Flynn, *Chem. Phys. Lett.* **56**, 429 (1978).
- ⁷C. W. von Rosenberg and D. W. Trainor, *J. Chem. Phys.* **59**, 2142 (1973).
- ⁸C. W. von Rosenberg and D. W. Trainor, *J. Chem. Phys.* **61**, 2442 (1974).
- ⁹C. W. von Rosenberg and D. W. Trainor, *J. Chem. Phys.* **63**, 5348 (1975).
- ¹⁰I. C. McDade and W. D. McGrath, *Chem. Phys. Lett.* **72**, 432 (1980).
- ¹¹I. C. McDade and W. D. McGrath, *Chem. Phys. Lett.* **73**, 413 (1980).
- ¹²S. M. Adler-Golden and J. I. Steinfeld, *Chem. Phys. Lett.* **76**, 479 (1980).
- ¹³S. M. Adler-Golden, E. L. Schweitzer, and J. I. Steinfeld, *J. Chem. Phys.* **76**, 2201 (1982).
- ¹⁴T. Kleindienst, J. B. Burkholder, and E. J. Bair, *Chem. Phys. Lett.* **70**, 117 (1980).
- ¹⁵J. A. Joens, J. B. Burkholder, and E. J. Bair, *J. Chem. Phys.* **76**, 5902 (1982).
- ¹⁶W. T. Rawlins, H. C. Murphy, G. E. Caledonia, J. P. Kennealy, F. X. Robert, A. Corman, and R. A. Armstrong, *Appl. Opt.* **23**, 3316 (1984).

- ¹⁷W. T. Rawlins, G. E. Caledonia, and J. P. Kennealy, *J. Geophys. Res.* **86**, 5247 (1981).
- ¹⁸W. T. Rawlins and R. A. Armstrong, *J. Chem. Phys.* **87**, 5202 (1987).
- ¹⁹W. T. Rawlins, G. E. Caledonia, J. J. Gibson, and A. T. Stair, Jr., *J. Geophys. Res.* **40**, 2896 (1985).
- ²⁰B. D. Green, W. T. Rawlins, and R. M. Nadile, *J. Geophys. Res.* **91**, 311 (1986).
- ²¹W. T. Rawlins, *J. Geophys. Res.* **90**, 12283 (1985).
- ²²D. L. Baulch, R. A. Cox, R. F. Hampson, Jr., J. A. Kerr, J. Troe, and R. T. Watson, *J. Phys. Chem. Ref. Data* **13**, 1259 (1984).
- ²³W. T. Rawlins, A. Gelb, and R. A. Armstrong, *J. Chem. Phys.* **82**, 681 (1985).
- ²⁴L. S. Rothman, R. R. Gamache, A. Barbe, A. Goldman, J. R. Gillis, L. A. Brown, R. A. Toth, J. M. Flaud, and C. Camy-Peyret, *Appl. Opt.* **22**, 2247 (1983).
- ²⁵R. E. Huie, J. T. Herron, and D. D. Davis, *J. Phys. Chem.* **76**, 2653 (1972).
- ²⁶I. Arnold and F. J. Comes, *Chem. Phys.* **42**, 231 (1979).
- ²⁷O. Klais, P. C. Anderson, and M. J. Kurylo, *Int. J. Chem. Kinet.* **12**, 469 (1980).
- ²⁸C. L. Lin and M. T. Leu, *Int. J. Chem. Kinet.* **14**, 417 (1982).
- ²⁹T. G. Slanger and G. Black, *J. Chem. Phys.* **70**, 3434 (1979).
- ³⁰F. Kaufman, *Adv. Chem. Ser.* **80**, 29 (1969).
- ³¹S. C. Brown, in *Encyclopedia of Physics, Vol. XXII Gas Discharges II*, edited by S. Flugge (Springer, Berlin, 1956), pp. 531-575.
- ³²R. D. Kenner and E. A. Ogryzlo, *Int. J. Chem. Kinet.* **12**, 501 (1980).
- ³³J. O. Hirschfelder, C. F. Curtiss, and R. B. Bird, *Molecular Theory of Gases and Liquids* (Wiley, New York, 1954).
- ³⁴M. Quack and J. Troe, *Ber. Bunsenges. Phys. Chem.* **79**, 179 (1975).
- ³⁵R. B. Bernstein and R. D. Levine, in *Advances in Atomic and Molecular Physics II*, edited by D. R. Bates and B. Bederson (Academic, New York, 1975), pp. 216-297; R. D. Levine and R. B. Bernstein, in *Modern Theoretical Chemistry, Vol. II: Dynamics of Molecular Collisions, Part B*, edited by W. H. Miller (Plenum, New York, 1975), Chap. 7.
- ³⁶J. P. Kennealy, F. P. Del Greco, G. E. Caledonia, and B. D. Green, *J. Chem. Phys.* **69**, 1574 (1978).
- ³⁷A. J. Stace and J. N. Murrell, *J. Chem. Phys.* **68**, 3028 (1978).
- ³⁸A. Gelb, *J. Phys. Chem.* **89**, 4189 (1985).
- ³⁹A. E. Croce de Cobos and J. Troe, *Int. J. Chem. Kinet.* **16**, 1519 (1984).
- ⁴⁰A. Gelb and W. T. Rawlins, Physical Sciences Inc., TR-567, under Air Force Contract No. F19628-85-C-0032, 1986.
- ⁴¹N. Swanson and R. J. Celotta, *Phys. Rev. Lett.* **35**, 783 (1975).
- ⁴²C. W. Wilson, Jr. and D. G. Hopper, *J. Chem. Phys.* **74**, 595 (1981).
- ⁴³L. S. Frost and A. V. Phelps, *Phys. Rev. A* **136**, 1538 (1969).
- ⁴⁴J. Dutton, *J. Phys. Chem. Ref. Data* **4**, 577 (1975).
- ⁴⁵L. J. Kieffer, JILA Information Center Report, September 30, 1973, Vol. 13.
- ⁴⁶S. A. Lawton and A. V. Phelps, *J. Chem. Phys.* **29**, 1055 (1978).
- ⁴⁷K. Tachibana and A. V. Phelps, *J. Chem. Phys.* **75**, 3315 (1981).
- ⁴⁸A. V. Phelps (private communication, 1982).
- ⁴⁹C. H. Jackman, R. H. Garvey, and A. E. S. Green, *J. Geophys. Res.* **82**, 5081 (1977).
- ⁵⁰J. W. Keto, *J. Chem. Phys.* **74**, 4445 (1981).
- ⁵¹J. Bretagne, J. Godart, and V. Peuch, *J. Phys. D* **15**, 2205 (1982).